Status Report on Mexican-Hat Flat-Topped Beams for Advanced LIGO

Erika D'Ambrosio,[1] Richard O'Shaughnessy,[2] Sergey Strigin,[3] Kip S. Thorne,[2] and Sergey Vyatchanin[3]

[1] *LIGO Laboratory, California Institute of Technology, Pasadena, CA 91125*
[2] *Theoretical Astrophysics, California Institute of Technology, Pasadena, CA 91125*
[3] *Physics Faculty, Moscow State University, Moscow, Russia*

(Dated: 23 January 2003)

LIGO Report Number LIGO-T030009-00-R

Summary

This document presents our conclusions and recommendations regarding the use of Mexican Hat (MH) mirrors and beams (a specific variant of *flat-topped beams*) in Advanced LIGO interferometers. We conclude that:

1. By switching from the baseline (BL) spherical mirrors and Gaussian beams to MH mirrors and beams with the same cylindrical test-mass diameters and thicknesses and the same diffraction losses, one can reduce the power spectral density of thermoelastic noise by a factor 0.34 and increase the event rate for compact-binary inspirals by a factor 2.6. Larger improvements could be achieved by using conical test masses with enlarged inner faces.

2. The sensitivity of the interferometer's arm cavities to transverse displacements of the ETMs is nearly the same for MH mirrors as for the BL spherical mirrors. For uncorrelated displacements of the ETM's through distances s, the fractions of the carrier power driven into (dipolar) parasitic modes inside the arm cavities, and driven out the dark port, are about $100(s/1\text{mm})^2$ ppm and $200(s/1\text{mm})^2$ ppm, respectively, for MH mirrors; and $100(s/1.3\text{mm})^2$ ppm and $200(s/1.3\text{mm})^2$ ppm for BL spherical mirrors.

3. The interferometer's arm cavities are about four times more sensitive to mirror tilt when MH mirrors are used than for the BL spherical mirrors. When all four ETM and ITM mirrors are tilted through angles θ about uncorrelated axes, the fractions of the carrier power driven into (dipolar) parasitic modes inside the arm cavities, and driven out the dark port, are about $0.001(\theta/0.01\mu\text{rad})^2$ and $0.002(\theta/0.01\mu\text{rad})^2$, respectively for MH mirrors; and $0.001(\theta/0.035\mu\text{rad})^2$ and $0.002(\theta/0.035\mu\text{rad})^2$ for BL mirrors.

4. For MH Mirror figure errors with peak-to-valley height variations Δz in the innermost 10 cm by radius: after the control system has optimized the mirror tilts, the fractions of the carrier power driven into parasitic modes inside the arm cavities, and driven out the dark port, are about $0.0008(\Delta z/6\text{nm})^2$ and $0.0015(\Delta z/6\text{nm})^2$, respectively.

5. The most serious constraints on mirror tilt and on mirror figure accuracy come not from the arm cavities but rather from the signal recycling (SR) cavity. The SR cavity and power recycling (PR) cavity operate approximately in the geometric optics regime and thus are nearly insensitive to whether one uses MH or spherical mirrors. As a result, by switching from spherical to MH mirrors, one pays only a small penalty, in terms of mirror tilt constraints and figure-error constraints.

6. More specifically, the most severe constraints on tilt and figure error arise from the driving of signal power into parasitic modes when the signal light passes through the SR cavity. To keep the resulting increase in shot noise below one per cent in the standard wideband Advanced-LIGO interferometers, it is necessary to constrain the magnitude θ of the vectorial tilts of the input test masses (ITM's) and signal recycling mirror (SRM) to $\theta^{\rm BL}_{\rm WB} \lesssim 0.024\mu$rad (for the baseline spherical mirrors) and $\theta^{\rm MH}_{\rm WB} \lesssim 0.016\mu$rad (for MH mirrors). For the third advanced interferometer, narrowbanded at $f \simeq 500$ Hz or $\simeq 1000$ Hz, the constraint must be tighter: $\theta^{\rm BL}_{\rm NB} \lesssim 0.011\mu$rad, and $\theta^{\rm MH}_{\rm NB} \lesssim 0.007\mu$rad. These are approximately the same as the well-known constraints on LIGO-I tilt arising from the PR cavity, in the absence of an output mode cleaner. If there is no output mode cleaner in Advanced LIGO, then the constraint on tilts in the PR cavity is about the same as that for wideband interferometers in the SR cavity. The increase in shot noise scales as θ^2; and we estimate that our constraints are inaccurate by a factor $\lesssim 2$ due to ignoring correlations in the overlaps of certain parasitic modes, and for the narrowbanded interferometers, due to inaccuracy of the geometric optics approximation in the SR cavity.

7. We characterize the analogous constraints on mirror figure error by the *peak-to-valley* fluctuations in the mirror height in the central regions of the mirrors (regions enclosing 95 per cent of the light power; radius $\simeq 10$ cm for MH mirrors and $\simeq 8$ cm for baseline spherical mirrors), with the fluctuations averaged over ~ 3 cm (an averaging produced by breakdown of geometric optics in the SR cavity). Our estimated constraints for one per cent increase of shot noise are $\Delta z_{\rm WB} \lesssim 2.0$ nm for wideband Advanced-LIGO interferometers and $\Delta z_{\rm NB} \lesssim 1.0$

nm for narrowband, independently of whether the mirrors are MH or BL spherical—though the region over which they must be applied is different, 10 cm radius for MH and 8 cm for BL. The increase in shot noise scales as Δz^2, and our estimated constraints might be inaccurate by as much as a factor ~ 3 due to exploring only one representative shape for the figure errors, due to overlaps of certain parasitic modes, and for the narrowbanded interferometer due to innacuracy of the geometric optics approximation in the SR cavity. These are approximately the same constraints as arise (in our calculations) from the PR cavity in LIGO-I, in the absence of an output mode cleaner. If there is no output mode cleaner in Advanced LIGO, then the constraint on tilts in the PR cavity is about the same as that for wideband interferometers in the SR cavity. To avoid these severe constraints, it may be desirable to shape the fronts of the ITM's as lenses that bring the light (Gaussian or MH) to a focus somewhere near the recycling mirrors; if this is done, the figures of the ITM fronts and/or the recycling mirrors presumably must be different in the MH case from the BL spherical case.

8. *The thermoelastic benefits of MH mirrors are sufficiently great, and the tightening of constraints that they place on mirror figures and tilts are sufficiently modest, to motivate carrying MH mirrors forward as an option for Advanced LIGO.*

9. As was discussed at the 6 September MIT meeting on flat-topped beams, a desirable next step is to determine the reproducibility and accuracy with which MH mirrors can be manufactured.

I. INTRODUCTION

We have proposed the use of flat-topped beams in LIGO-II to reduce thermelastic noise in the mirrors' sapphire substrates [1–5]. Arm-cavity mirrors that support these beams have faces (mirror figures) that resemble mexican hats. The mirrors and beams are thus called *Mexican-Hat* or *MH* mirrors and beams.

We gave detailed results of our modeling on MH mirrors and beams, as of early September 2002, in a preliminary draft of a paper for Physical Review D [5], and in a presentation at a meeting on this subject at MIT [4]. A number of practical issues were raised by the participants in the MIT meeting. We have investigated many of those issues. This report summarizes the results of those recent investigations (Sec. IV) and also, for completeness, summarizes the most important of our earlier conclusions (Secs. II and III). Plans and recommendations for future research are discussed in Sec. V.

II. REDUCTION OF THERMOELASTIC NOISE

Independent of whether MH mirrors are incorporated into LIGO-II, we recommend that the mirror coatings be extended out to the outer edge of the test-mass faces rather than stopping 8 mm short of the edge, and that the beams be enlarged accordingly, limited only by holding the diffraction losses at their baseline level. (The quality of the coating can be lower in the outer regions without much penalty, because so little power resides there.) This change will permit enlarging the baseline radius of the Gaussian beam, at the mirrors, from 4.23 cm to 4.49 cm (Table 1 of [5]), resulting in a reduction of the power spectral density of thermoelastic noise by a factor 0.856, an increase in the range for the LIGO-II network to see NS/NS binary inspirals from 300 Mpc to 315 Mpc (Table V of [5]) and similarly for NS/BH and BH/BH, and a corresponding increase in the event rate for inspirals of $(315/300)^3 = 1.16$. *In what follows, we shall assume this revised baseline for LIGO-II with spherical mirrors and Gaussian beams.*

How much reduction of thermoelastic noise can we achieve by switching from this new Gaussian baseline ($r_o = 4.49$ cm; thin curve in bottom panel of Fig. 1) to an MH beam with the same 10 ppm diffraction losses on the same 15.7 cm × 13 cm test masses (MH radius parameter $D/b = 3.73$ in the notation of [5]; thick curve in bottom panel of Fig. 1)? Independent computations by three of us (SS, SV and RO'S) have shown that this switch to MH beams reduces the power spectral density of thermoelastic noise by a further factor 0.34

$$\frac{S_h^{\text{TE, MH}}}{S_h^{\text{TE, Gaussian}}} \simeq 0.34 \qquad (2.1)$$

(in [5] compare the second entry in Table I with the sixth entry in Table II). *If other thermal noises are negligible*, this increases the distance to which the LIGO network can see NS/NS binary inspirals from 315 Mpc to 431 Mpc (Table V of [5]), and similarly for NS/BH and BH/BH binaries; and correspondingly it increases the event rate for inspiraling binaries by about $(431/315)^3 \simeq 2.6$:

$$\frac{\text{Inspiral Rate with MH beams}}{\text{Inspiral Rate with Gaussian beams}} \simeq 2.6\,. \qquad (2.2)$$

It is possible to achieve further substantial noise reductions and sensitivity gains by giving the mirrors and beams larger diameters or, at fixed mirror mass, by switching to conically shaped mirrors [4, 5].

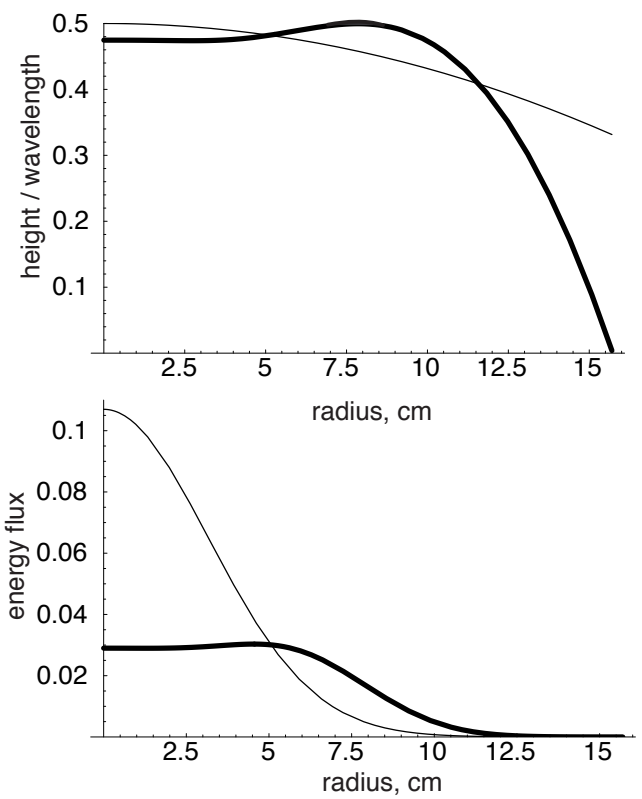

FIG. 1: Bottom panel: the energy fluxes $|u_0|^2$ (normalized to unity, $\langle u_0, u_0\rangle = \int |u_0|^2 d\text{Area} = 1$) for the MH beam (thick curve) and Gaussian beam (thin curve) that have 10 ppm of diffraction losses on a mirror with coated radius 15.7 cm. Top panel: the shapes of the MH and spherical mirrors that support these beams. The MH mirror is significantly flatter than the spherical mirror in the central 10 cm radius where most of the light power is contained, but is much steeper outside there.

III. PRACTICAL ISSUES: SUMMARY OF RESULTS REPORTED AT THE MIT MEETING

A. Parameter Values for Comparing MH and BL Configurations

When analyzing practical issues, we have carried out most of our computations for fiducial MH mirrors that have slightly larger coated radii, $R_M = 16$cm, than the baseline Advanced-LIGO mirrors (14.9 cm at present and 15.7 cm if our recommendation to coat the outer 8 mm is followed), and we have used MH beams with modestly larger diffraction loss, $\mathcal{L}_0 = 18$ ppm, than the current baseline of about 10 ppm. In evaluating practical issues in this report we will compare with baseline spherical mirrors and Gaussian beams that have this same enlarged coated radius $R_M = 16$ cm and diffraction loss $\mathcal{L}_0 = 18$ ppm.

Our mirror and beam parameters, then, are as follows: For the baseline (BL) configuration, mirror radius $R_M = 16$ cm (vs 15.7 cm for the true current baseline) and Gaussian beam radius $r_o = 4.70$ cm (vs. 4.23 cm for the true current baseline); and for the MH configuration, mirror radius $R_M = 16$ cm and beam radius parameter $D = 4b = 10.4$ cm, where $b = \sqrt{\lambda L/2\pi} = 2.60$ cm, with $\lambda = 1.06\mu$m and $L = 4$km the light wavelength and arm length. (In Ref. [5] we used the true current baseline $r_o = 4.23$ cm in our comparisons, so the baseline constraints on tilts quoted in this report differ from those there by a factor of order 10 per cent.)

B. Driving an MH Interferometer with a Gaussian Beam

One way to produce the MH beams is to drive the interferometer with Gaussian-beam light and let the arm cavities or a mode-cleaning cavity convert the light into MH form. One of us, ED'A, has identified the Gaussian beam that has the greatest overlap with the MH beam of an arm cavity. If one were to drive the MH arm cavity directly with a Gaussian beam, this would be the driving beam one would want to use. It has a beam radius $r_{od} = 6.92$ cm, compared to our baseline cavity's beam radius at the ITM of $r_o = 4.70$ cm. This Gaussian driving beam $u_d(r)$ has an overlap

$$\gamma_0^2 \equiv |\langle u_0|u_d\rangle|^2 \equiv \left|\int u_0^* u_d d\text{Area}\right|^2 = 0.940 \qquad (3.1)$$

with the cavity's fundamental MH mode u_0, which means that 94.0 per cent of the Gaussian driving-beam light will enter the cavity, and 6.0 per cent will get rejected. See Ref. [6] and Sec. VB of [5].

C. Parasitic Modes in Arm Cavities

It is useful to think of the MH mirrors as having two regions: a central region with radius $\simeq 10$ cm, and an outer region with radius $\simeq 6$ cm. In its central region, the MH mirror is much flatter than the baseline spherical mirror; in its outer region, it is much more sharply curved; see the top panel of Fig. 1. The flatness of the central region has led to concerns about degeneracies of modes and sensitivity to tilt and to figure errors.

One of us (RO'S) has solved the integral eigenequation for the modes of a LIGO arm cavity with MH mirrors. He found (slide 15 of [4] and Table VI of [5]), and SS and SV have verified independently, that *among modes that are not strongly damped by diffraction losses, the one closest in frequency to the fundamental TEM00 mode u_0 is the lowest TEM01 mode (denoted u_1 below). Its frequency separation from the fundamental is 0.0404 of the cavity's free spectral range, which is 2.5 times smaller than our baseline Gaussian cavity's* $0.099 \times$ *(free spectral range).* Evidently, the sharp curvature of the MH mirrors' outer region compensates sufficiently for the flatness of their

central region, to prevent the parasitic modes' frequencies from becoming near degenerate with the fundamental.

D. Mirror Tilt in Arm Cavities

As we have reported before [4, 5], our modeling predicts that *the mode mixing in the arm cavities of a MH interferometer produced by tilt of the ETM's or ITM's should be of no serious consequence, if the tilt angles are kept below about* 10^{-8} *rad.* In the following subsections we summarize the calculations that lead to this conclusion.

1. Parasitic mode mixing in arm cavities

Two of us have computed the influence of a tilt of the ETM on the fundamental mode of an arm cavity: ED'A has done this using an FFT code, and RO'S has done it by applying perturbation theory to the arm cavity's integral eigenequation. The two computations agree on the following predictions:

When the ETM is tilted through an angle θ, the cavity's fundamental mode gets changed from $u_0(r)$ to

$$u_0'(\vec{r}) = (1-\alpha_1^2/2)u_0(r) + \alpha_1 u_1(\vec{r}) + \alpha_2 u_2(\vec{r}) \ . \quad (3.2)$$

Here $\vec{r}$ is position in the transverse plane, u_n are unit-norm superpositions of modes of the perfectly aligned cavity ($\int |u_n|^2 d\text{Area} = 1$), α_n are mode-mixing coefficients that scale as θ^n, and our computations have been carried out only up through quadratic order. The maximum tilt that can be allowed is of order 10^{-8} radian, so we shall express our predictions for the α_n in units of $\theta_8 \equiv \theta/10^{-8}$.

For our baseline Gaussian-beam cavity, u_0 is the (0,0) Hermite-Gaussian mode, u_1 is the (0,1) Hermite Gaussian mode, u_2 is the (0,2) mode, and the dominant mixing coefficient α_1 is

$$\alpha_1^{\rm BL} = \frac{1}{\sqrt{2}(1-g^2)^{3/4}} \left(\frac{\theta^{\rm BL}}{b/L}\right) = 0.0064\theta_8 \quad (3.3)$$

(Eq. (5.24) of [5]). Here $g = 0.952$ is our BL arm cavity's g-factor and $b = \sqrt{\lambda L/2\pi} = 2.60$ cm is its transverse diffraction scale. For the MH cavity, maps of u_0, u_1, and u_2 are shown in Figs. 6 and 7 of [5] and slide 17 of [4]; and the mixing coefficients are

$$\alpha_1^{\rm MH} = 0.0227\theta_8 \ , \quad \alpha_2^{\rm MH} = 0.00018\theta_8^2 \quad (3.4)$$

(Eqs. (5.22) and (5.23) of [5] and slide 18 of [4]). Comparison of Eqs. (3.3) and (3.4) shows that, *to keep the dominant, dipolar mode-mixing coefficient* α_1 *at the same level in the MH cavity as in the baseline Gaussian-beam cavity requires controlling the MH mirrors' tilt angle* θ *four times more tightly.*

The fractional power in the dominant, dipolar parasitic mode is α_1^2, which will be doubled to

$$\begin{aligned} P_1^{\text{BL arm total}} &\simeq 2(\alpha_1^{\rm BL})^2 \simeq 0.001(\theta_8/3.5)^2 \ , \\ P_1^{\text{MH arm total}} &\simeq 2(\alpha_1^{\rm MH})^2 \simeq 0.001\theta_8^2 \ , \end{aligned} \quad (3.5)$$

when the ITM and ETM are both tilted but about uncorrelated axes. This *suggests that, so far as the arm cavities are concerned (i.e., ignoring issues of tilt in the recycling cavities), the tilt of MH mirrors need not be controlled much better than* $\simeq 10^{-8}$ *rad.* We have verified this by examining the effects of the mode mixing on various cavity and interferometer parameters:

2. Diffraction Losses

One of us (ED'A), from her FFT simulations [6], has estimated the influence of ETM tilt on diffraction losses to be

$$\mathcal{L}_0'^{\rm MH} = \mathcal{L}_0^{\rm MH}(1 + 0.004\theta_8^2) \ . \quad (3.6)$$

(This result been confirmed to a factor ~ 2 by RO'S by combining the clipping approximation with perturbation theory of the cavity's eigenequation; Eq. (5.26) of [5] and slide 19 of [4]).

The influence of ITM tilt should be about the same, thus doubling the coefficient of θ_8^2. *This tilt-induced increase in losses is so small that it can be ignored for tilt angles below* $\sim 10^{-8}$ *rad.*

3. Arm Cavity Gain

We have computed (ED'A via the FFT code and RO'S via perturbation theory) the following influence of ETM tilt on the arm cavity gain

$$G_{\rm cav}^{\rm MH} = 740(1 - 0.00057\theta_8^2) \ . \quad (3.7)$$

(Eq. (5.31) of [5]; slide 19 of [4]). This result assumes the baseline values for the power transmissivities of the ITM and ETM, which we approximate as $|t_I|^2 = 0.005$, $|t_E|^2 = 0$, and assumes for simplicity that the only losses are diffraction losses. The factor 740 assumes the cavity is driven by its best-fit Gaussian beam and thus is smaller by about $\gamma_0^2 = 0.940$ than the gain in the (untilted) baseline cavity. The tilt of the ITM should produce about the same gain reduction as that of the ETM, thus doubling the coefficient of θ_8^2 to ~ 0.001. This coefficient is small enough that *the tilt-induced decrease of MH arm-cavity gain will be negligible if* θ *is controlled to* $\sim 10^{-8}$ *rad.*

4. Dark Port Power

We have computed the influence of the tilt of one ETM on the dark-port output light (ED'A using the FFT code

and RO'S using perturbation theory). We find for the fraction of the interferometer's input power that winds up at the dark port in the fundamental mode u_0 and the parasitic modes u_1 and u_2:

$$\begin{aligned} P_0^{\text{MH DP}} &= 0.26\theta_8^4 \text{ ppm} , \\ P_1^{\text{MH DP}} &= \gamma_0^2\alpha_1^2 = 480\theta_8^2 \text{ ppm} , \\ P_2^{\text{MH DP}} &= \gamma_2^2\alpha_2^2 = 0.024\theta_8^4 \text{ ppm} \end{aligned} \tag{3.8}$$

(Eqs. (5.38)–(5.41) of [5] and slide 20 of [4]). With all four cavity mirrors being tilted about uncorrelated axes, the dark-port powers should be four times larger than this,

$$\begin{aligned} P_0^{\text{MH DP total}} &\simeq 1.0\theta_8^4 \text{ ppm} , \\ P_1^{\text{MH DP total}} &\simeq 2000\theta_8^2 \text{ ppm} , \\ P_2^{\text{MH DP total}} &\simeq 0.1\theta_8^4 \text{ ppm} \end{aligned} \tag{3.9}$$

Without an output mode cleaner, the dark-port power will primarily be in the dipolar mode u_1, and for $\theta < 10^{-8}$ rad it will constitute < 0.2 per cent of the input light. An output mode cleaner will wipe out this u_1 power and the power in mode u_2, leaving only the tiny fundamental-mode power, which should be totally negligible for θ below 10^{-8} rad.

For comparison, the dark-port powers with the baseline Gaussian beams are

$$\begin{aligned} P_0^{\text{MH DP total}} &\simeq 1.0(\theta_8/3.5)^4 \text{ ppm} , \\ P_1^{\text{MH DP total}} &\simeq 2000(\theta_8/3.5)^2 \text{ ppm} , \end{aligned} \tag{3.10}$$

which shows once again that the BL arm cavities are ~ 4 times less sensitive to tilt than the MH arm cavities.

IV. PRACTICAL ISSUES: NEW RESULTS SINCE THE MIT MEETING

A. Transverse Displacement of Arm Cavities' Mirrors

When the ETM is displaced transversely through a distance s, the cavity's fundamental mode gets changed from $u_0(r)$ to

$$u_0'(\vec{r}) = (1 - \zeta_1^2/2)u_0(r) + \zeta_1 w_1(\vec{r}) + \zeta_2 w_2(\vec{r}) , \tag{4.1}$$

where the parasitic modes w_n, like the u_n's, have unit norm, $\langle w_n|w_n\rangle = \int |w_n|^2 d\text{Area} = 1$, and have phase adjusted so the coupling coefficients ζ_n are real, and where $\zeta_n \propto s^n$.

R'OS has computed the coupling coeffients ζ_n for the BL spherical mirrors and for MH mirrors by applying perturbation theory to the cavity's eigenequation. In both cases ζ_2 is negligible compared to ζ_1 when the displacement is $s \ll b \equiv \sqrt{\lambda L/2\pi} = 2.60$ cm, so we shall ignore ζ_2. R'OS finds that the MH and BL mirrors are roughly equally sensitive to transverse displacements; their coupling coefficients are

$$\begin{aligned} \zeta_1^{\text{BL}} &= \left(\frac{(1-g)^{1/4}}{\sqrt{2}(1+g)^{3/4}}\right)\frac{s}{b} = 0.008 s_{\text{mm}} , \\ \zeta_1^{\text{MH}} &= 0.010 s_{\text{mm}} . \end{aligned} \tag{4.2}$$

Here $g = 0.952$ is the BL arm cavity's g-factor, and s_{mm} is the ETM's transverse displacement in millimeters.

The corresponding fraction of the arm-cavity carrier power driven into the (dipolar) parasitic field w_1 is

$$P_1^{\text{arm total}} = \zeta_1^2 \simeq \begin{cases} 100(s/1.3\text{mm})^2\text{ppm} & \text{BL}, \\ 100(s/1.0\text{mm})^2\text{ppm} & \text{MH}. \end{cases} \tag{4.3}$$

The fraction of the input carrier power driven out the dark port when the ETMs of both arm cavities are displaced through a distance s but in uncorrelated directions is about twice the above:

$$P_1^{\text{DP total}} = 2\gamma_0^2\zeta_1^2 \simeq \begin{cases} 190(s/1.3\text{mm})^2\text{ppm} & \text{BL}, \\ 190(s/1.0\text{mm})^2\text{ppm} & \text{MH}. \end{cases} \tag{4.4}$$

These coupling coefficients and parasitic-mode powers are sufficiently small that we presume transverse displacements are not a serious issue, and so shall ignore them in the rest of this report. In any event, the low sensitivity to a change from BL spherical to MH mirrors makes displacement a non-issue in the decision about MH mirrors.

B. Errors in the Arm Cavities' Mirror Figures

1. Billingsley's Worst-Case Figure Error

Garilynn Billingsley has provided us with a map of a worst-case figure error, $\delta z_{\text{wc}}(x, y)$ [height error as function of Cartesian coordinates in the transverse plane], produced by current technologies. Her map is based on the measured deviation of a LIGO-I beam-splitter substrate from flatness. The measured substrate had diameter 25 cm; she stretched its deviation from flatness (its "figure map") to the baseline mirror diameter of 35.4 cm, fit Zernike polynomials to the stretched map, and smoothed the map by keeping only the lowest 36 Zernikes.

We show a contour diagram of the resulting figure map (figure "error") in Fig. 2. In the central region (innermost 10 cm in radius), the peak to valley error Δz is about 30 nm, while in the outer region (10 cm to 16 cm in radius), it is about 110 nm. Billingsley thinks it likely that in the central region (which dominates our considerations), peak-to-valley errors of $\Delta z \sim 5$ nm may be achievable — about 1/5 as large as in Fig. 2; and we have found that $\Delta z = 0.2 \times 30 = 6$ nm is small enough that the influences of the figure error scale, for $\delta z \lesssim 6$ nm, as Δz or Δz^2 with higher-order terms producing $\lesssim 10$ per cent

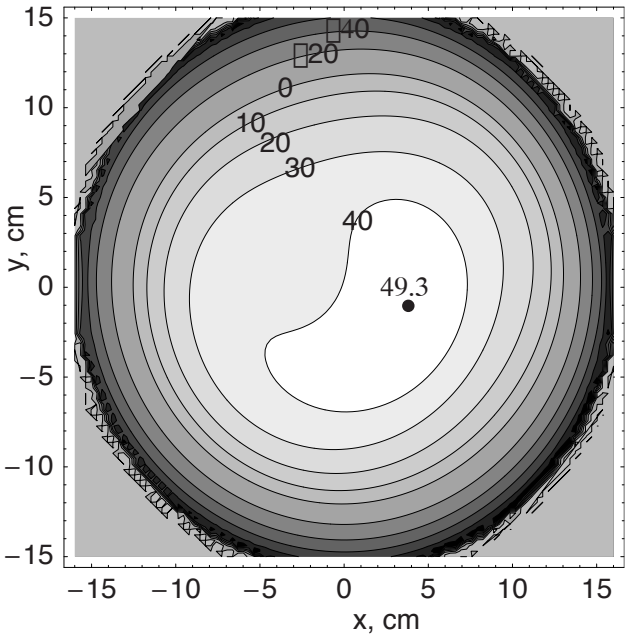

FIG. 2: Contour diagram of Billingsley's worst-case figure error [height $\delta z_{\rm wc}$ in nanometers as a function of transverse Cartesian coordinates (x, y) in centimeters]. The hash at the outer edge of the mirror is an artifact of our numerical manipulation of Billingsley's map.

corrections. Accordingly, in the analyses described below we shall use Billingsley's map, scaled down in height by a factor ε:

$$\delta z = \varepsilon \delta z_{\rm wc}(x, y) \ , \tag{4.5}$$

and we shall use $\varepsilon = 0.2$ and $\Delta z = 6$ nm as our fiducial values for ε and Δz. Jean Marie Mackowski believes that $\Delta z \sim 2$ nm errors may be achievable if the mirror figure is produced by coating; this corresponds to $\varepsilon \sim 0.07$.

2. *Mode Mixing by Figure Errors Without Compensating Tilt*

We have computed the mode mixing in an MH cavity when Billingsley's worst-case figure error reduced by $\varepsilon \lesssim 0.2$ is placed on the ETM. As in our tilt studies, the computation was done independently by ED'A using the FFT code and by RO'S using arm-cavity perturbation theory.

By analogy with Eq. (3.2), the fundamental mode with deformed ETM has the following form

$$u_0' = (1 - \beta_1^2/2)u_0 + \beta_1 v_1 \ , \tag{4.6}$$

where the parasitic mode v_1, like the u_n's, has unit norm $\langle v_1 | v_1 \rangle = \int |v_1|^2 d\text{Area} = 1$, and has a phase adjusted so that $\beta_1 \propto \varepsilon/0.2$ is real. By contrast with the tilt-induced mode mixing, where u_1 is dipolar (angular dependence $\cos\varphi$), the deformation parasite v_1 has a complicated shape that depends on the details of the deformation and that therefore contains a number of multipoles. A map of the power distribution $|\beta_1 v_1|^2$ of the admixed mode is shown in Fig. 3.

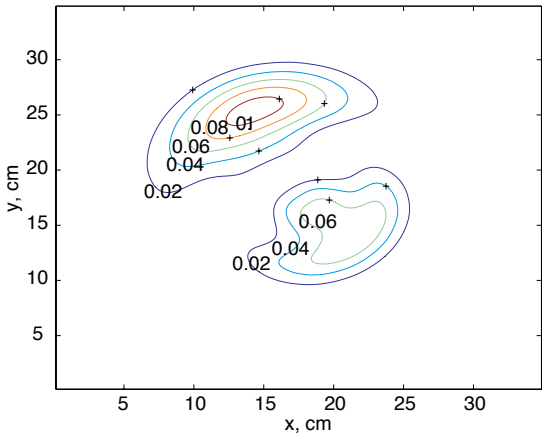

FIG. 3: The power distribution $|u_0' - u_0|^2 = |\beta_1 v_1|^2$ (in units $1/\text{m}^2$) of the deformation-induced parasitic mode when the deformation $\varepsilon \delta z_{\rm wc}(x, y)$ with $\varepsilon = 0.2$ is applied to the ETM of an MH arm cavity. This map was computed by ED'A using the FFT code; the map computed by RO'S using perturbation theory is in reasonable agreement with this one (e.g., the heights of the two peaks are $\{0.111, 0.080\}$ in the FFT map, and $\{0.110, 0.088\}$ in the perturbation map. The parasitic power $|\beta_1 v_1|^2$ scales as $(\varepsilon/0.2)^2$.

The fraction of the arm cavity power in the parasitic mode is

$$P_1^{\text{MH arm}} = \beta_1^2 = 0.0012(\varepsilon/0.2)^2 \ , \tag{4.7}$$

and the fraction of the interferometer's input power that goes out the dark port (if the interferometer is driven by the best-fit Gaussian mode u_d and if only one of the arm mirrors — one ETM — is deformed) is given by

$$P_1^{\text{MH DP}} = \gamma_0^2 \beta_1^2 = 0.0011(\varepsilon/0.2)^2 \tag{4.8}$$

At the leading, ε^2, order in the deformation (the order to which we have computed), this dark-port power is entirely in the parasitic mode v_1. Our FFT and perturbation-theory calculations agree on the parasitic powers (4.7) and (4.8) to within about five per cent.

The dark-port power (4.8) and parasitic arm-cavity power (4.7) are influenced primarily by the figure error in the central (10 cm radius) region of the ETM, because about 96 per cent of the MH-mode power is contained in that central region, and only about 4 per cent in the outer region — and of the outer 4 per cent, 3/4 (3 per cent) is in the annulus between 10 and 11 cm. The insensitivity to outer region deformations is fortunate, because Billingsley tells us that it will be much easier to keep the figure errors small in the central region than in the outer region.

[RO'S has verified the insensitivity to the outer-region deformations by evaluating (via perturbation theory) the dark-port power for a mirror deformation

$$\delta z = \varepsilon_c \delta z_{\rm wc}^{\rm central} + \varepsilon_o \delta z_{\rm wc}^{\rm outer} \ . \qquad (4.9)$$

Here $\delta z_{\rm wc}^{\rm central}$ is equal to $\delta z_{\rm wc}$ at $r < 9.6$ cm and is zero at $r > 12.2$ cm, and between 9.6 and 12.2 cm, $\delta z_{\rm wc}^{\rm central}/\delta z_{\rm wc}$ falls linearly from 1 to zero; and similarly $\delta z_{\rm wc}^{\rm outer}$ is equal to $\delta z_{\rm wc}$ at $r > 12.2$ cm and is zero at $r < 9.6$ cm, and between 9.6 and 12.2 cm $\delta z_{\rm wc}^{\rm outer}/\delta z_{\rm wc}$ grows linearly from 0 to 1. RO'S finds, as a function of the central-region and outer-region weightings,

$$P_1^{\rm MH\ DP} = \gamma_0^2 \beta_1^2 = 0.0010(\epsilon_c/0.2)^2 + 1.5\times 10^{-5}(\epsilon_o/0.2)^2; \qquad (4.10)$$

so that, for example, if Billingsley's worst-case perturbations are reduced by $\epsilon_c = 0.2$ in the central region (to $\Delta z = 6$ nm), but are kept at their full original strength $\epsilon_o = 1.0$ in the outer region (so $\Delta z = 110$ nm there), the outer region will contribute 40 per cent as much power to the dark port as the inner region.]

When all four arm-cavity mirrors are subjected to uncorrelated deformations, the arm-cavity parasitic power (4.7) will be increased by a factor 2 and the dark-port power (4.8) by a factor 4, to

$$\begin{aligned} P_1^{\rm MH\ arm\ total} &\simeq 0.0025(\Delta z/6{\rm nm})^2 \ , \\ P_1^{\rm MH\ DP\ total} &\simeq 0.005(\Delta z/6{\rm nm})^2 \end{aligned} \qquad (4.11)$$

where Δz is the peak-to-valley mirror deformation in the central region. This suggests that, *so far as arm-cavity mode mixing is concerned, peak-to-valley figure errors of order 6 nm in the inner 10 cm are acceptable.*

3. Mode Mixing by Figure Errors With Compensating Tilt

The parasitic mode v_1 (Fig. 3) contains a significant amount of dipolar field, as one sees from the asymmetry of the map. The LIGO-II tilt control system, based on a quadrant-diode readout of asymmetry in the power distribution u_0', will tilt the mirror so as to remove the overlap between the deformed parasitic field v_1 and the dipolar-tilt parasitic field u_1. ED'A and R'OS have independently computed that the optimal tilt is about $\theta_{\rm compensate} = 1.3 \times 10^{-8}(\varepsilon/0.2)$ radians about a line rotated 55 degrees from the x axis, and have computed the resulting field $u_0' = u_0 + \beta_1 v_1 + \alpha_1 u_1$ with minimum parasitic-mode power. Figure 4 shows the mirror deformation after tilt, and Fig. 5 shows the parasitic power distribution $|\beta_1 v_1 + \alpha_1 u_1|^2$ for $\varepsilon = 0.2$. Notice that the tilt has largely but not completely removed the dipolar asymmetry. Some residual dipolar field remains — that portion which cannot be compensated by a tilt.

We denote by v_{1c} the tilt-compensated parasitic mode and by β_{1c} its (real) amplitude, so $\beta_{1c} v_{1c} = \beta_1 v_1 + \alpha_1 u_1$. Then the cavity's eigenmode, with tilt compensation (including the second-order loss of power from u_0) is

$$u_0' = (1 - \beta_{1c}^2/2) u_0 + \beta_{1c} v_{1c} \ , \qquad (4.12)$$

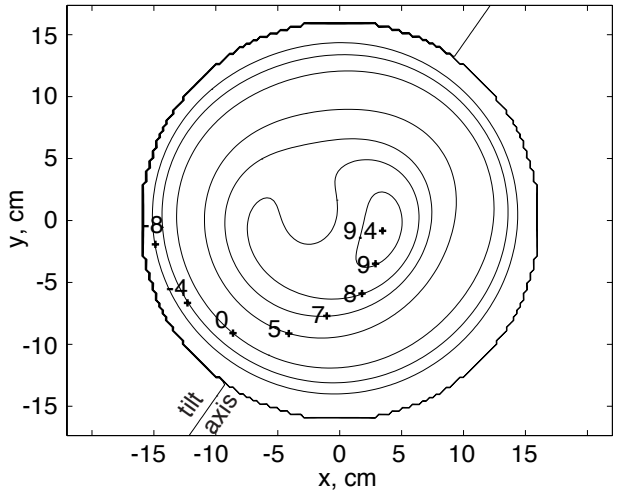

FIG. 4: Billingsley's worst-case figure error reduced by a factor $\epsilon = 0.2$, when the mirror is tilted to optimally reduce the MH beam's odd-parity power: $\delta z = 0.2\delta z_{\rm wc} + \theta_{\rm compensate} \sin(\varphi - 55^{\rm o})]$. The numbers on the contours are height in nanometers.

and optimization of the tilt compensation gives for the fraction of the power in the parasitic mode

$$P_{1c}^{\rm MH\ arm} = \beta_{1c}^2 = 0.00040(\varepsilon/0.2)^2 = 0.00040(\Delta z/6{\rm nm})^2 \ . \qquad (4.13)$$

The fraction of the interferometer's input power that goes out the dark port (all in the parasitic modes), after this tilt compensation, is

$$P_1^{\rm MH\ DP} = \gamma_0^2 \beta_{1c}^2 = 0.00038(\varepsilon/0.2)^2 \ . \qquad (4.14)$$

Comparing with Eq. (4.8), we see that *the figure-error-induced power out the dark port is reduced by a factor* 3 *by the compensating tilt of the deformed mirror.*

The dark-port power (4.14) is for an interferometer with one deformed MH arm mirror. When all four mirrors are deformed in uncorrelated ways, the arm-cavity parasitic power will be doubled and the dark-port power will be quadrupled:

$$\begin{aligned} P_1^{\rm MH\ arm\ total} &\simeq 0.0008(\Delta z/6{\rm nm})^2 \ , \\ P_1^{\rm MH\ DP\ total} &\simeq 0.0015(\Delta z/6{\rm nm})^2 \ . \end{aligned} \qquad (4.15)$$

This suggests that, so far as arm-cavity mode mixing is concerned, we could live with central region deformations as large as 10 nm. Recycling-cavity issues, discussed below, will place much tighter constraints on the mirror figures.

C. Influence of Mirror Tilt and Figure Errors on Thermoelastic Noise

When one MH mirror of an arm cavity is given the deformation $\varepsilon \delta z_{\rm wc}$, the resulting deformation of the arm-

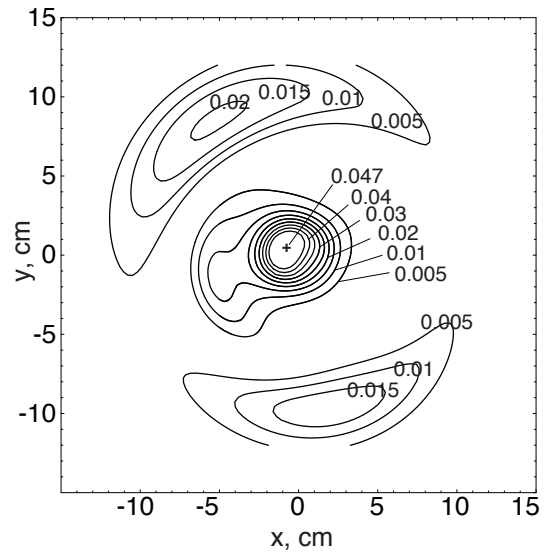

FIG. 5: The power distribution $|u_0' - u_0|^2 = |\beta_{1c} v_{1c}|^2$ (in units $1/\mathrm{m}^2$) of the deformation-induced parasitic mode when the tilt-adjusted deformation $\delta z = 0.2\delta z_{\rm wc} + \theta_{\rm compensate} \sin(\varphi - 55^\circ)]$ is applied to the ETM of an MH arm cavity. This map was computed by RO'S by applying perturbation theory to the cavity's eigenmode. The map computed by ED'A using the FFT code agrees reasonably well.

cavity power distribution, $\delta|u_0'|^2 = |u_0'|^2 - |u_0|^2$ increases the thermoelastic noise. The following argument (due to R'OS) shows that, at leading (linear) order in $\varepsilon/0.2$, *only the circularly symmetric portion of the parasitic mode* $\beta_1 v_1 = u_0' - u_0$ *contributes to the thermoelastic noise increase*: The fractional noise increase is equal to the fractional increase in the thermoelastic noise integral $I = \int (\vec{\nabla}\Theta)^2 d\mathrm{vol}$ (Eq. (4.2) of [5]; slide 6 of [4]):

$$\frac{\delta S_h^{\rm TE\ MH}}{S_h^{\rm TE\ MH}} = \frac{\delta I}{I} \propto \int (\vec{\nabla}\Theta)\cdot(\vec{\nabla}\delta\Theta) d\mathrm{vol}\ . \qquad (4.16)$$

Here Θ is not a tilt angle but rather is the expansion (fractional increase of volume) of the substrate material when a static pressure $P \propto |u_0'|^2$ is applied to the mirror face. Since the unperturbed MH beam is circularly symmetric, so will be the unperturbed expansion Θ, which means that only the circularly symmetric portion of the expansion perturbation $\delta\Theta$, and thence the circularly symmetric portion of the pressure perturbation $\delta P \propto \delta|u_0'|^2$ will contribute to the noise increase. At leading (linear) order in the mirror deformation $\varepsilon/0.2$, the circularly symmetric portion of $\delta|u_0'|^2$ arises solely from the circularly symmetric portion of $\delta u_0' = \beta_1 v_1$; thus, as claimed, only the circularly symmetric portion of $\beta_1 v_1$ can increase the thermoelastic noise.

This same argument shows that *the MH mode deformation produced by mirror tilt cannot influence the thermoelastic noise at first order in the tilt angle*; and therefore, *we need not be concerned about the influence of tilt on the thermoelastic noise — whether the tilt is unintended, or is being used in a controlled way to compensate the errors in the mirror figures.*

RO'S has evaluated and SS has confirmed the fractional increase in the thermoelastic noise integral at linear order in $\varepsilon/0.2$. The result, multiplied by four to account for four arm-cavity mirrors, is

$$\frac{\delta S_h^{\rm TE,\ MH\ total}}{S_h^{\rm TE,\ MH}} = 0.14(\varepsilon/0.2) \simeq 0.14(\Delta z/6\mathrm{nm})\ . \qquad (4.17)$$

This 14 per cent increase of S_h, when all four mirrors are subjected to 6 nm figure errors in their central regions, is to be compared with the factor $1/0.35 = 285$ *per cent decrease in thermoelastic noise achieved by switching from spherical mirrors to MH mirrors.* There may also be a small increase in thermoelastic noise when a spherical mirror is deformed. *Assuming, conservatively, no deformation-induced noise increase for spherical mirrors, switching from spherical to 6nm-deformed MH mirrors will reduce the thermoelastic noise by a factor* $0.34 \times 1.14 = 0.39$*, which in turn will increase the distance for NS/NS binaries from 315 Mpc to about 425 Mpc and increase the event rate by about a factor 2.45* (Fig. 5 of [5]).

D. MH vs. Gaussian Beams in Recycling Cavities

The greatest worries raised at the MIT meeting on flat-topped (MH) beams were those related to the power recycling and signal recycling cavities. In the baseline design, (which has *no* lenses in the recycling cavities), these cavities are already so nearly degenerate that major problems are anticipated from mode mixing due to mirror deformations (both static deformations and inadequately compensated deformations by thermal lensing). There was great worry that for MH mirrors, with their greater central-region flatness, this already severe mode mixing might be made substantially worse.

We have examined this question and conclude that *for the two wideband Advanced-LIGO interferometers, there is not much difference between the baseline Gaussian beams and the proposed MH beams, with regard to their susceptibility to mode mixing in the recycling cavities.* The only significant difference arises from the fact that the MH beams are larger and therefore sample, with significant power, larger-radii regions of the mirrors (the regions between, say, 8 cm radius and 10 cm radius), where the deformations may be worse.

The reason that the mode mixing is only marginally sensitive to the beam shape is quite simple: Once RF modulated sideband light gets into the power recycling cavity, it makes roughly $\mathcal{N}_{\rm PR} \sim \frac{1}{2}$(cavity finesse $\mathcal{F}_{PR}$) $\simeq (\pi/2)/(1 - R_{\rm PR}) \simeq 25$ round trips before losing 95 per cent of its power out the beam splitter's dark port. (Here $R_{\rm PR} \simeq 0.94$ is the power reflectivity of the power recycling mirror). And once signal light

gets into the signal recycling cavity, it makes roughly $\mathcal{N}_{\rm SR} \sim \frac{1}{2}\pi/(1-\rho\sqrt{R}) \sim 40$ round trips before losing 95 per cent of its power out the dark port or back into the arm cavities. (Here $R = 0.995$ is the ETM power reflectivity and $\rho = \sqrt{0.93}$ is the amplitude reflectivity of the SR mirror, in the notation of Buonanno and Chen [7].) The Fresnel length (transverse diffraction scale) for light that makes $\mathcal{N}$ round trips in either recycling cavity with cavity length $\ell \simeq 10$ m is

$$r_F = \sqrt{\lambda_o 2\ell\mathcal{N}} \simeq 3{\rm cm}\sqrt{\mathcal{N}/40}\,, \tag{4.18}$$

where $\lambda_o = 1\mu$m is the light's wavelength. This Fresnel length is $\sim 1/2$ of the ~ 5 cm scales on which the ideal mirror shapes and the central-region worst-case mirror errors vary, and it is small compared to the $\sim$ 15 to 20 cm diameter beams themselves. There thus is only modest diffractive coupling between light rays, and *the light bouncing back and forth in each recycling cavity is describable, to moderately good accuracy, by geometric optics.* Moreover, because the mirrors (whether MH or spherical) are nearly flat and nearly identical, the light's rays, to rather good accuracy, are all parallel to the optic axis and to each other and are thus decoupled from each other. If the mirrors and beam splitter were perfect and ideal in shape, the extreme length of their radii of curvature, $\gtrsim 50$ km, compared to the optical pathlength in the recycling cavities, $2\ell\mathcal{N} \lesssim 1$ km, would guarantee that the MH beam would resonate equally well in the ideal MH-mirrored cavity or in the ideal spherical-mirrored cavity, or in a precisely flat-mirrored cavity; and the baseline Gaussian beam would also resonate, equally well, in all these cavities.

If the third interferometer is operated in narrow-band mode, then the number of round trips the signal light makes in the SR cavity will be much larger than 40, and the geometric optics approximation will begin to fail significantly. More specifically, for ETM reflectivity $R = 0.995$ and optimized narrow banding at {500 Hz, 1000 Hz}, the SR mirror's amplitude reflectivities are $\rho = \{0.994, 0.9985\}$ [see discussion following Eq. (4.25) below], corresponding to a number of round trips in the SR cavity $\mathcal{N}_{\rm SR} \simeq \{180,\ 400\}$ and Fresnel lengths $r_F \simeq \{6{\rm cm},\ 9{\rm cm}\}$. These Fresnel lengths (the transverse scale for diffractive light spreading) are about 1/3 to 1/2 the 95-percent-power diameter of the beam, 16 cm (BL) and 20 cm (MH). As we shall see below, this means that geometric optics can be used to get a rough upper limit on the fractional increase in shot noise due to tilt and irregularities of the SR cavity's mirrors, but not a reliable estimate of the shot-noise increase.

E. Increase in Shot Noise Due to Mirror Tilts

1. Foundations

The mirror tilts produce a mismatch between various modes of the light, thereby increasing the shot noise. We shall focus on the shot noise increase at the minimum of the signal light's optical resonance in the arm cavity. This optical resonance is the one that is used to produce a noise minimum for a narrow-banded Advanced LIGO interferometer, and it is the right-hand minimum of the optical noise for the standard wide-band Advanced LIGO interferometer, and approximately the minimum of the wide-band interferometer's total noise.

The (unit-norm) modes whose mismatch increases the shot noise are the following:

1. u_0, the eigenmode of perfect arm cavities.
2. u'_0, the carrier's eigenmode in an arm cavity with tilted ITM and ETM.
3. u'_s, the signal field's eigenmode in an arm cavity, at the center of its optical resonance, with tilted ITM, ETM, and SRM (signal recycling mirror).
4. u'_t, the field produced when u_0 is transmitted through the signal recycling cavity with tilted ITM and SRM.
5. u'_r, the reference-light field that is beat against the signal light to produce the input to the photodetector. We focus on the case of RF readout, so u'_r is the side-band light transmitted through the power recycling cavity to the photodetector, and its distortions are produced by the tilt of the ITM and PRM (power recycling mirror).

For each primed field u'_ℓ, we denote by δ_ℓ the fraction of its light power that is in parasitic modes and thus has been lost from the fundamental mode u_0 due to mirror tilt:

$$\langle u_0, u'_\ell\rangle^2 = 1 - \delta_\ell\ . \tag{4.19}$$

The signal amplitude entering the photodetector is proportional to

$$S \propto \langle u'_r, \tilde\tau' u'_s\rangle\langle u'_s, u'_0\rangle\langle u'_0, u_d\rangle\ . \tag{4.20}$$

The sequence of terms, from right to left, have the following meanings, and we approximate them as follows:

1. $\langle u'_0, u_d\rangle$ describes the influence of tilts on the driving of the arm cavity's eigenmode by the Gaussian driving field. For simplicity, we neglect the tiny coupling of the driving field to the second-order parasitic mode u_2 contained in u_0 and therefore approximate this coupling amplitude by $\langle u'_0, u_d\rangle = \gamma_0\langle u'_0, u_0\rangle = \gamma_0(1-\alpha_{1E}^2/2 - \alpha_{1I}^2/2) = \gamma_0(1-\delta_0/2)$. Here the subscripts I and E denote the contributions from the tilts of the ITM and ETM.
2. $\langle u'_s, u'_0\rangle$ describes the influence of tilts on the driving of the arm cavity's signal field by its carrier field (via the gravitational-wave-induced motion of the mirrors). For simplicity we neglect the (nonzero) overlap between the parasitic modes contained in u'_s and u'_0, thereby obtaining $\langle u'_s, u'_0\rangle = (1 - \delta_s/2 - \delta_0/2)$.

3. $\langle u'_r, \tilde{\tau}' u'_s\rangle$ describes the influence of tilts on (i) the passage of the signal u'_s, through the SR cavity (with cavity transmissivity $\tilde{\tau}'$ in the notation of Buonanno and Chen [7]), and on (ii) the overlap of the transmitted signal light with the reference light to produce the photodetector current. Again we neglect correlations between the parasitic components of the fields and therefore approximate the influence of the tilts by $\langle u'_r, \tilde{\tau}' u'_s\rangle \propto (1-\delta_r/2-\delta_s/2-\delta_t/2)$. The δ_j terms represent the loss of overlap due to the parasitic-mode fields (assumed uncorrelated) contained in u'_r (the δ_r term), contained in u'_s (the δ_s term), and generated by the passage of the signal light through the SR cavity, whose mirror tilts deform the transmissivity $\tilde{\tau}'$, (the δ_t term).

If there is no mode cleaner on the interferometer output, then the rms amplitude of the shot noise is $N \propto \sqrt{\langle u'_r, u'_r\rangle} = 1$; i.e. the parasitic-mode components of u'_r contribute to the rms noise amplitude along with the fundamental-mode component. However, a mode cleaner will remove the parasitic components, so that $N \propto \langle u_0, u'_r\rangle = 1 - \delta_r/2$.

Combining the above approximations to the various terms, we find for the ratio of noise power to signal power (which is proportional to the spectral density of shot noise $S_h^{\rm shot}$ at the minimum of the optical resonance):

$$S_h^{\rm shot} \propto \frac{N^2}{|S|^2} \propto 1+2\delta_0+2\delta_s+\delta_t+\begin{cases}\delta_r\ , & \text{no mode cleaner}\\ 0 & \text{with mode cleaner.}\end{cases} \tag{4.21}$$

(Note that we have ignored the increase in shot noise due to carrier-light parasitic fields going out the dark port, Eqs. (3.9) and (4.15), under the assumption that it is negligible, either because of an output mode cleaner or because the arm-cavity-mirror figures and tilts are adequately controlled.)

We shall now examine the various contributions to the shot noise one by one.

2. Carrier Light in Arm Cavity

The fraction of the arm-cavity carrier light that is driven into parasitic modes by tilts of the ETM and ITM is $\delta_0 = \alpha_{1E}^2 + \alpha_{1I}^2$. The loss of this carrier light to parasites increases the shot noise by

$$\left(\frac{\delta S_h^{\rm shot}}{S_h^{\rm shot}}\right)^{\rm MH}_{\rm carrier} = 2\delta_0 = 4\alpha_1^2 = 0.01\left(\frac{\theta}{2\times 10^{-8}}\right)^2 . \tag{4.22}$$

Here we have assumed that both mirrors are tilted through the same angle θ but about uncorrelated axes, we have assumed MH beams, and we have used Eq. (3.4) for α_1. The baseline Gaussian beams are four times less sensitive to tilt, so to keep this contribution to the spectral density of shot noise below one per cent, we must control the ITM and ETM tilts to an accuracy

$$\theta^{\rm MH}_{1\%} = 2\times 10^{-8}\ , \quad \theta^{\rm BL}_{1\%} = 8\times 10^{-8}\ . \tag{4.23}$$

These are modest constraints on tilt.

3. Signal Light in Arm Cavity

The signal recycling (SR) cavity presents a complex amplitude reflectivity $\tilde{\rho}' = e^{-\epsilon/F}e^{i\lambda/F}$ to the arm cavity's signal light (Eqs. (5) and (13) of Buonanno and Chen [7]). Here $F = c/2L$ is the interferometer's free spectral range, $\epsilon = \epsilon(R,\rho,\phi)$ and $\lambda = \lambda(R,\rho,\phi)$ are real functions of the ITM power reflectivity R, the SRM amplitude reflectivity ρ and the SR cavity's tuning phase $\phi = (k\ell)_{\rm mod 2\pi}$, with ℓ the length of the cavity; and our notation is that of Buonanno and Chen [7]. Tilts of the ITM and SRM produce a spatially variable reflectivity $\tilde{\rho}'$. The spatial variations of the modulus $e^{-\epsilon/F}$ of $\tilde{\rho}'$ presumably will have much less influence on the arm cavity's signal eigenmode u'_s than the spatial variations of the phase. (This claim deserves to be checked.) Assuming this is so, then the dominant influence of an ITM or SRM tilt θ is to produce a spatially variable mirror displacement

$$\delta z = \theta r \sin\varphi \tag{4.24}$$

(where φ is azimuthal angle and r is radius), which in turn (*in the SR cavity's geometric optics limit*) produces a spatially variable phase of the cavity reflectivity, $\arg(\tilde{\rho}') = \delta\lambda/F = (d\lambda/d\phi)(k/F)\delta z$. If the cavity were replaced by a single mirror that is displaced through a distance $\delta z_{\rm eff}$, then this phase change would be $2k\delta z_{\rm eff}$. Correspondingly, the tilt of the ITM or SRM produces an effective mirror displacement $\delta z_{\rm eff} = \mathcal{A}\delta z$, where the amplification factor $\mathcal{A}$ is given by

$$\mathcal{A} = \frac{\delta z_{\rm eff}}{\delta z} = \frac{d\lambda/d\phi}{2F} = (1-R)\rho\frac{2\rho+(1+\rho^2)\cos 2\phi}{(1+\rho^2)+2\rho\cos 2\phi}\ ; \tag{4.25}$$

see Eq. (18) of Buonanno and Chen [7].

We shall focus on three configurations for the SR cavity: (i) The standard wideband Advanced-LIGO configuration (denoted "WB"), for which $R = 0.995$, $\rho = \sqrt{0.93}$, and $\phi = \pi/2 - 0.06$. (ii) An interferometer narrowbanded at a frequency $f = \lambda/2\pi \simeq 500$ Hz with bandwidth $\Delta f = \epsilon/2\pi \simeq 50$ Hz, which has a noise minimum of $\simeq 1\times 10^{-24}/\sqrt{\rm Hz}$; this configuration (which we shall denote "500") is produced by $R = 0.995$, $\rho = 0.994$, and $\phi = 1.541$. (iii) An interferometer narrowbanded at $f = \lambda/2\pi \simeq 1000$ Hz with bandwidth $\Delta f = \epsilon/2\pi \simeq 50$ Hz (and so denoted "1000"), which has a noise minimum of $\simeq 1\times 10^{-24}/\sqrt{\rm Hz}$ and parameters $R = 0.995$, $\rho = 0.9985$, $\phi = 1.556$. For these three configurations the amplification factor is

$$\mathcal{A}_{\rm WB} = 0.27\ , \quad \mathcal{A}_{500} = 1.4\ , \quad \mathcal{A}_{1000} = 5.7\ . \tag{4.26}$$

We have chosen to compute the shot noise increase at the optical resonance so the signal field u'_s in the arm cavity will be on resonance, just as the carrier field is. This allows us to translate our carrier-field results over to the signal field with only one change: the influence of the tilts of the SRM and ITM must be multiplied by the amplification factor $\mathcal{A}$. Therefore, the fraction δ_s of the signal field's power that is in the tilt-induced parasitic modes is $\delta_s = \alpha_{1E}^2 + \mathcal{A}^2(\alpha_{1I}^2 + \alpha_{1SR}^2)$. The influence α_{1E}^2 of the ETM is the same as in the case of the carrier, which we have already dealt with, so we shall ignore it here and focus on the two mirrors that make up the SR cavity: the ITM and the SRM. If they both have the same tilt angles θ (but about uncorrelated axes) so $\alpha_{1I}^2 = \alpha_{1SR}^2 \equiv \alpha_1^2$, then these tilts produce a fractional increase in shot noise given by

$$\left(\frac{\delta S_h^{\rm shot}}{S_h^{\rm shot}}\right)_{\rm signal} = 2\delta_s = 4\mathcal{A}^2\alpha_1^2 \ . \qquad (4.27)$$

This is greater by the factor $\mathcal{A}^2$ than the noise (4.22) due to loss of carrier light into parasitic modes, and correspondingly to keep this fractional increase of shot noise below one per cent requires controlling the ITM and SRM tilts to an accuracy $1/\mathcal{A}$ of that in Eq. (4.23):

$$\begin{aligned} \theta_{1\%}^{\rm MH\ WB} &= 7\times10^{-8}\ , \quad \theta_{1\%}^{\rm BL\ WB} = 30\times10^{-8}\ , \\ \theta_{1\%}^{\rm MH\ 500} &\gtrsim 1.4\times10^{-8}\ , \quad \theta_{1\%}^{\rm BL\ 500} \gtrsim 6\times10^{-8}\ , \\ \theta_{1\%}^{\rm MH\ 1000} &\gtrsim 0.4\times10^{-8}\ , \quad \theta_{1\%}^{\rm BL\ 1000} \gtrsim 1.4\times10^{-8}\ . \end{aligned} \qquad (4.28)$$

For the narrow-banded interferometers these limits are only lower bounds on $\theta_{1\%}$ because of the failure of the geometric optics limit. As we have seen, the Fresnel length for light trapped in the SR cavity is about 1/2 to 1/3 of the 95-percent-power beam diameter, so transverse spreading of the light will reduce somewhat the SR cavity's amplification factor $\mathcal{A}$ and thence the influence of tilt on the beam asymmetry. We *guess* that this reduction might increase $\theta_{1\%}^{1000}$ by a factor of order 2 over the geometric-optics limit, (4.28); but since $\mathcal{A}$ is only about 1 for $\theta_{1\%}^{1000}$, we *guess* that there is little increase in $\theta_{1\%}^{500}$; so

$$\begin{aligned} \theta_{1\%}^{\rm MH\ 500} &\simeq 1.4\times10^{-8}\ , \quad \theta_{1\%}^{\rm BL\ 500} \simeq 6\times10^{-8}\ , \\ \theta_{1\%}^{\rm MH\ 1000} &\simeq 0.8\times10^{-8}\ , \quad \theta_{1\%}^{\rm BL\ 1000} \simeq 3\times10^{-8}\ . \end{aligned} \qquad (4.29)$$

4. *Transmission of Signal Light Through SR Cavity*

When the ITM or SRM is tilted through an angle θ, producing a spatially dependent mirror displacement $\delta z = \theta r \sin\varphi$, it alters the SR cavity's transmissivity by a spatially dependent amount $\delta\tilde\tau' = (d\tilde\tau'/d\phi)k\delta z$, *in the geometric optics limit*. When an undistorted signal beam u_0 passes through this spatially variable transmissivity, a fraction

$$\langle u_0, |\delta\tilde\tau'/\tilde\tau'|^2 u_0\rangle = \frac{1}{2}\mathcal{B}^2k^2\langle r^2\rangle\theta^2\ . \qquad (4.30)$$

gets transferred to parasitic modes. Here $k = 2\pi/\lambda_o$ is the wave number, $\langle r^2\rangle = \langle u_0, r^2u_0\rangle$ is the beam's mean square radius, which has the values

$$\begin{aligned} \langle r^2\rangle &= (6.95{\rm cm})^2 \quad \text{for MH beam} \\ \langle r^2\rangle &= r_o^2 = (4.70{\rm cm})^2 \quad \text{for BL Gaussian beam,} \end{aligned} \qquad (4.31)$$

and

$$\mathcal{B}^2 = \left|\frac{d\tilde\tau'/d\phi}{\tilde\tau'}\right|^2 = \frac{4R\rho^2}{1+R\rho^2+2\sqrt{R}\rho\cos2\phi}\ . \qquad (4.32)$$

Here we have used Eq. (11) of Buonanno and Chen [7] for $\tilde\tau'$, with the factor $e^{i\phi(\vec r)}$ in the numerator removed, so as to obtain the transmissivity that carries the field from an input transverse plane to an output transverse plane in the presence of the mirror tilt (which gives ϕ its dependence on transverse position $\vec r$). For our three interferometer configurations, the values of $\mathcal{B}$ are

$$\mathcal{B}_{\rm WB} = 15\ , \quad \mathcal{B}_{500} = 33\ , \quad \mathcal{B}_{1000} = 66\ . \qquad (4.33)$$

When both ITM and SRM are tilted through the same angle θ about uncorrelated axes, the total power transferred into parasitic modes is twice as large as Eq. (4.30) [i.e., δ_t is twice (4.30)], and correspondingly the fractional increase in shot noise is

$$\left(\frac{\delta S_h^{\rm shot}}{S_h^{\rm shot}}\right)_{\rm transmission} = \delta_t = \mathcal{B}^2k^2\langle r^2\rangle\theta^2\ . \qquad (4.34)$$

Inserting the above values for B and $\langle r^2\rangle$ and insisting that the shot noise not increase by more than one per cent, we obtain the following constraints on the ITM and SRM tilt angles:

$$\begin{aligned} \theta_{1\%}^{\rm MH\ WB} &= 1.6\times10^{-8}\ , \quad \theta_{1\%}^{\rm BL\ WB} = 2.4\times10^{-8}\ , \\ \theta_{1\%}^{\rm MH\ 500} &\gtrsim 0.7\times10^{-8}\ , \quad \theta_{1\%}^{\rm BL\ 500} \gtrsim 1.1\times10^{-8} \\ \theta_{1\%}^{\rm MH\ 1000} &\gtrsim 0.4\times10^{-8}\ ; \quad \theta_{1\%}^{\rm BL\ 1000} \gtrsim 0.6\times10^{-8}\ . \end{aligned} \qquad (4.35)$$

For the narrow-banded interferometers, the failure of the geometric optics limit dictates that these estimates of $\theta_{1\%}$ are lower limits; hence the "$\gtrsim$". As in the case of signal light in an arm cavity reflecting off the SR cavity, so also here, we *guess* that these estimates are fairly good for narrow banding at 500 Hz and are roughly a factor 2 too severe at 1000 Hz, so

$$\begin{aligned} \theta_{1\%}^{\rm MH\ 500} &\simeq 0.7\times10^{-8}\ , \quad \theta_{1\%}^{\rm BL\ 500} \simeq 1.1\times10^{-8} \\ \theta_{1\%}^{\rm MH\ 1000} &\simeq 0.7\times10^{-8}\ ; \quad \theta_{1\%}^{\rm BL\ 1000} \simeq 1.1\times10^{-8}\ . \end{aligned} \qquad (4.36)$$

Equations (4.35) for wideband interferometers and (4.36) for narrowband are the most severe of all our tilt constraints.

5. Transmission of RF reference light through power recycling cavity

Suppose that the PRM or ITM is tilted through an angle θ and is thereby given the space-dependent displacement $\delta z = \theta r \sin\varphi$. Then, in the geometric optics limit, the RF reference light acquires, when passing through the PR cavity, a space-dependent phase shift $(\mathcal{F}/\pi)k\delta z$, where $\mathcal{F}$ is the cavity finesse. The reference light emerging from the cavity therefore has the form $u'_r = u_0 e^{i(\mathcal{F}/\pi)k\delta z}$, for which the fraction of light power in parasitic modes is

$$\left\langle u_0, \left(\frac{\mathcal{F}}{\pi}\right)^2 k^2 \delta z^2 \, u_0 \right\rangle = \frac{1}{2}\left(\frac{\mathcal{F}}{\pi}k\right)^2 \langle r^2\rangle\theta^2 \, . \quad (4.37)$$

When both the PRM and the ITM are tilted through the same angle θ but around uncorrelated axes, the parasitic mode power is twice as large [so δ_r is twice (4.37)], and the fractional increase in shot noise due to the loss of this reference-light power is then

$$\left(\frac{\delta S_h^{\rm shot}}{S_h^{\rm shot}}\right)_{\rm reference} = \delta_r = \left(\frac{\mathcal{F}}{\pi}k\right)^2 \langle r^2\rangle\theta^2 \, . \quad (4.38)$$

For the LIGO-I interferometers $\mathcal{F}$ is rather large, $\mathcal{F} \simeq 125$, which produces a strong sensitivity to mirror tilt; but for Advanced LIGO $\mathcal{F}$ is smaller, $\mathcal{F} \simeq 50$, which (as we shall see) compensates for the larger beam, thereby producing about the same sensitivity to tilt as for LIGO-I.

Inserting the LIGO-I finesse $\mathcal{F} \simeq 125$ and mean square beam radius $\langle r^2\rangle = b^2 = (2.6\text{cm})^2$, and constraining the shot noise increase to less than one per cent, we obtain the following constraint on the ITM and PRM tilts:

$$\theta_{1\%}^{\rm LIGO-I} \simeq 1.6\times 10^{-8} \, . \quad (4.39)$$

This is in remarkably good agreement with a much more careful computation by Fritschel et. al. [8], which gave[1] $\theta_{1\%}^{\rm LIGO-I} = 1.4\times 10^{-8}$.

Inserting the LIGO-II finesse $\mathcal{F} \simeq 50$ and mean-square beam radius $\langle r^2\rangle = (6.95\text{cm})^2$ (MH) and $(4.70\text{cm})^2$ (BL), and constraining the increase in shot noise to no more than one per cent, we obtain

$$\theta_{1\%}^{\rm MH} \simeq 1.5\times 10^{-8} \, , \quad \theta_{1\%}^{\rm BL} \simeq 2.5\times 10^{-8} \, ,$$

As we have seen, an output mode cleaner will remove this shot noise increase, making these (rather modest) constraints no longer needed.

[1] Their result (end of Sec. 2.A) is $\theta < 1.0\times 10^{-8}$ for the tilts in pitch and in yaw, corresponding to a constraint $\theta < \sqrt{2}\times 10^{-8} \simeq 1.4\times 10^{-8}$ on the magnitude of the vectorial tilt, for an 0.005 fractional decrease in amplitude signal to noise, which corresponds to our one per cent increase in S_h.

F. Increase in Shot Noise Due to Mirror Figure Errors

The increase in spectral density of shot noise due to mirror figure errors is given by the same equation $S_h^{\rm shot} \propto 1 + 2\delta_0 + 2\delta_s + \delta_t + \{\delta_r \text{ or } 0\}$ as for mirror tilt [Eq. (4.21)], but now δ_ℓ is the fraction of power in the parasitic components of mode u'_ℓ due to figure errors rather than tilt.

1. Carrier light in arm cavity

Deformations of the ITM and ETM, with optimized tilt compensation, drive a fraction $\delta_0 = \beta_{1cE}^2 + \beta_{1cI}^2$ into parasitic modes [Eqs. (4.12) and (4.13)]. Assuming the same peak-to-valley deformations Δz in the two mirrors' central regions, we obtain for the fractional increase in shot noise

$$\left(\frac{\delta S_h^{\rm shot}}{S_h}\right)^{\rm MH} = 2\delta_0 = 4\beta_{1c}^2 \simeq 0.01\left(\frac{\Delta z}{15\text{nm}}\right)^2 \, . \quad (4.40)$$

Correspondingly, to keep the shot noise increase below one per cent, we must constrain the ITM and ETM deformations to

$$\Delta z_{1\%}^{\rm MH} \simeq 15\text{nm} \quad (4.41)$$

We have not carried out an analysis of the influence of the ITM and SRM mirror deformations on the baseline Gaussian arm cavity modes, and so cannot say what the analogous constraint is in the baseline case.

2. Signal light in arm cavity

As for tilt, so also for figure errors, the SR cavity amplifies the influence of the errors Δz by a factor $\mathcal{A}$ [Eq. (4.25)], so the ITM and SRM deformations move a fraction $\delta_s = \mathcal{A}^2(\beta_{1c\,I}^2 + \beta_{1c\,SR}^2)$ of the arm cavity's signal light into parasitic modes. When the two figure errors have the same magnitude and we wish to keep the resulting shot noise increase below one per cent, this gives rise to constraints on the ITM and SRM figure errors that are $1/\mathcal{A}$ more severe than (4.41). Using the values (4.26) of $\mathcal{A}$ for our three interferometers (wide-band, narrow-banded at 500 Hz and narrow-banded at 1000 Hz), and increasing the limit for the 1000-Hz narrow-banded case by a factor 2 due to failure of the geometric-optics limit [cf. Eq. (4.29) and associated discussion], we obtain the constraints

$$\begin{aligned} \Delta z_{1\%}^{\rm MH\ WB} &\simeq 55\text{nm} \, , \\ \Delta z_{1\%}^{\rm MH\ 500} &\gtrsim 10\text{nm} \, , \text{ with a guess of } \simeq 10\text{nm} \, , \\ \Delta z_{1\%}^{\rm MH\ 1000} &\gtrsim 2.6\text{nm} \, , \text{ with a guess of } \simeq 5\text{nm} \, . \end{aligned} \quad (4.42)$$

3. Transmission of signal light through SR cavity

By the same analysis as for mirror tilt (Sec. IV E 4), deformations $\delta z(x,y)$ of the ITM and SRM by the same peak-to-valley amounts Δz produce an increase in shot noise given by

$$\left(\frac{\delta S_h^{\rm shot}}{S_h^{\rm shot}}\right)_{\rm transmission} = \delta_t = 2\mathcal{B}^2k^2\langle(\delta z)^2\rangle\theta^2 = \frac{1}{4}\mathcal{B}^2k^2(\Delta z)^2 \qquad (4.43)$$

[cf. Eq. (4.34) with $\langle(\delta z)^2\rangle = \langle(\theta r\sin\varphi)^2\rangle = \frac{1}{2}\langle r^2\rangle\theta^2$]. Here $\langle(\delta z)^2\rangle$ is the mean square deviation of ITM or SRM height from the desired figure, and we have approximated this by half the squared amplitude of mirror height fluctuations, which is 1/8 the square of the peak to valley height fluctuations, $(\Delta z)^2/8$. Inserting the values of $\mathcal{B}$ for our three interferometers [Eq. (4.33)] and requiring that the shot noise increase by no more than one per cent, we obtain the following constraints on the ITM and SRM peak to valley deformations:

$$\begin{aligned}\Delta z_{1\%}^{\rm MH\ WB} &= \Delta z_{1\%}^{\rm BL\ WB} \simeq 2{\rm nm},\\ \Delta z_{1\%}^{\rm MH\ 500} &= \Delta z_{1\%}^{\rm BL\ 500} \lesssim 1{\rm nm},\ \text{with a guess} \simeq 1{\rm nm}\ ,\\ \Delta z_{1\%}^{\rm MH\ 1000} &= \Delta z_{1\%}^{\rm BL\ 1000} \lesssim 0.5{\rm nm},\ \text{with a guess} \simeq 1{\rm nm}\ .\end{aligned} \qquad (4.44)$$

Here as in Eqs. (4.42), (4.36) and (4.29), the breakdown of the geometric optics limit in the SR cavity has dictated a lower limit and a guess for the narrowbanded interferometers.

These are the most serious of our constraints on the mirror figures of advanced interferometers, and they are the same for MH and baseline Gaussian beams, because transmission through the SR cavity is governed (at least roughly) by geometric optics. The one small difference is that the central region over which the peak-to-valley deformations are constrained (the region containing ~ 95 per cent of the light power) is larger for MH mirrors (central radius about 10 cm) than for the baseline Gaussian mirrors (central radius about 8 cm).

The mirror figure constraint (4.44) is sufficiently severe, at least in the case of narrow-banded interferometers, that it might be worth considering reducing the degeneracy of the SR cavity by making the entrance faces of the ITM's into lenses that bring the signal light (and inevitably also the carrier light) to a focus somewhere near the SRM (and PRM). Since the constraint (4.44) is the same, whether the mirrors are MH or spherical, this recommendation is not dependent on whether MH beams are implemented.

4. Transmission of RF reference light through power recycling cavity

By the same argument as for mirror tilt (Sec. IV E 5), in the absence of a mode cleaner, deformations $\delta z(x,y)$ of the ITM and PRM produce a net shot noise increase given by

$$\left(\frac{\delta S_h^{\rm shot}}{S_h^{\rm shot}}\right)_{\rm reference} = \delta_r = 2\left(\frac{\mathcal{F}}{\pi}k\right)^2\langle(\delta z)^2\rangle = \frac{1}{4}\left(\frac{\mathcal{F}}{\pi}k\right)^2(\Delta z)^2 \qquad (4.45)$$

[cf. Eq. (4.38) with $\langle(\delta z)^2\rangle = \langle(\theta r\sin\varphi)^2\rangle = \frac{1}{2}\langle r^2\rangle\theta^2$]. Inserting the finesses of LIGO-I ($\mathcal{F}\simeq 125$) and Advanced LIGO ($\mathcal{F}\simeq 50$) and insisting that the shot noise not be increased by more than one per cent, we obtain the following constraints on the central-region peak-to-valley deformations of the PRM and SRM:

$$\begin{aligned}\Delta z_{1\%}^{\rm LIGO-I} &= 0.8{\rm nm}\ ,\\ \Delta z_{1\%}^{\rm MH} &= \Delta z_{1\%}^{\rm BL} = 2{\rm nm}\ ,\end{aligned} \qquad (4.46)$$

The LIGO-I constraint is rather severe, but can be removed by using an output mode cleaning cavity. The Advanced LIGO constraint is less severe, and can also be relaxed by an output mode cleaner.

V. RECOMMENDED RESEARCH RESEARCH BY THE LSC

The thermoelastic benefits of MH mirrors are sufficiently great, and the tightened constraints that they place on mirror figures and tilts are sufficiently modest, that *we recommend MH mirrors be adopted by the LSC as an option for Advanced LIGO, and be incorporated into future modeling along with spherical mirrors.*

Among the issues that the LSC may wish to examine are these:

1. As we have discussed in Sec. IV D, the constraints on mirror figure in the recycling cavities are very worrisome. Detailed studies of this seem needed. As one aspect of these studies, it would be worthwhile to check our geometric-optics-based claims that the MH recycling cavities are not much more sensitive to mirror figure errors than the baseline Gaussian-beam cavities. If the constraints on mirror figure are found to be as serious as our estimates suggest, then it seems worthwhile to carry out studies of the option of converting the input faces of the ITM's into lenses that make the recycling cavities much less degenerate. Such studies are needed (and presumably are under way), in any event, for LIGO-I, where our estimated PR-cavity constraints are even more severe than in Advanced LIGO [Eqs. (4.46)].

2. Bill Kells (at the MIT meeting on flat topped beams) suggested the possibility of operating the Advanced LIGO interferometers with spherical mirrors and Gaussian beams, and later switching

to MH beams by altering only the ETM's. It seems to us that this option is worth detailed study. If the ITM input faces are turned into lenses that reduce the near degeneracy of the recycling cavities, then it might be possible to keep the lenses weak enough that the figures of the recycling mirrors can be the same for Gaussian and MH beams, while still relaxing the mirror figure constraints to an acceptable level. This needs study.

3. Braginsky, in a private conversation, has pointed out that the substrate shapes can change, due to stress-induced readjustment of their internal structures, by amounts of order 0.1 to 0.01 microradians on times of weeks. This, like thermal lensing, may necessitate monitoring and maintaining the desired mirror figures using, e.g., heating via CO_2 lasers.

Acknowledgments

For helpful discussions and advice we thank, among others, Raymond Beausoleil, Garilynn Billingsley, Alessandra Buonanno, Vladimir Braginsky, Yanbei Chen, Peter Fritschel, Bill Kells, David Shoemaker, Robert Spero, Ken Strain, Rai Weiss, Phil Willems, Stan Whitcomb, Farid Khalili, Mike Zucker, and especially Garilynn Billingsley. This research was supported in part by NSF grants PHY-0098715 and PHY–0099568, by the Russian Foundation for Fundamental Research grants #96-02-16319a and #97-02-0421g, and (for SPV) by the NSF through Caltech's Institute for Quantum Information.

[1] E. d'Ambrosio, R. O'Shaughnessy, and K. Thorne, LIGO Report Number LIGO-G000223-00-D (16 August 2000).
[2] V. Braginsky, E. d'Ambrosio, R. O'Shaughnessy, S. Strigin, K. Thorne, and S. Vyatchanin, LIGO Report Number LIGO-G010151-00-R (16 March 2001).
[3] V. Braginsky, E. d'Ambrosio, R. O'Shaughnessy, S. Strigin, K. Thorne, and S. Vyatchanin, LIGO Report Numbers LIGO-G010333-00-D and LIGO-010297-00-D (15 August 2001).
[4] V. Braginsky, E. d'Ambrosio, R. O'Shaughnessy, S. Strigin, K. Thorne, and S. Vyatchanin, LIGO Report Number LIGO-G020543-00-R (6 September 2002).
[5] E. d'Ambrosio, R. O'Shaughnessy, S. Strigin, K. Thorne, and S. Vyatchanin, Phys. Rev. D (2000), in preparation; available as the file beamreshape020903.pdf at http://www.cco.caltech.edu/∼kip/ftp/.
[6] E. D'Ambrosio, Phys. Rev. D (2003), submitted.
[7] A. Buonanno and Y. Chen, Phys. Rev. D (2002), submitted; gr-qc/0208048.
[8] P. Fritschel, N. Mavalvala, D. Shoemaker, D. Sigg, M. Zucker, and G. Gonzalez, Applied Optics **37**, 6734 (1998).